

Flow Angularity and Swirl Flow Analysis on Transonic Compressor Rotor by 1-Dimensional Dynamic Turbine Engine Compressor Code and CFD Analysis

M. U. Sohail^{a,b,*}, H. R. Hamdani^{a,**}, and K. Parvez^{a,***}

^a Department Aerospace and Aeronautics, Institute of Space Technology, Islamabad, 46000, Pakistan

^b Department Mechanical Engineering, National University of Technology (NUTECH), Islamabad, Pakistan

*e-mail: engr.mu.sohail@gmail.com

**e-mail: hrza@hotmail.com

***e-mail: khalidparvez2009@hotmail.com

Received January 17, 2020; revised March 17, 2020; accepted June 21, 2020

Abstract—The performance and stability of a low-bypass turbofan transonic axial compressor with a nonuniform inlet flow is a significant concern in recent times. In both military and commercial aircraft, serpentine ducts produce significant inlet swirl distortion. Moreover, the nonuniform inlet flow frequently acts upon aircraft gas-turbine engines causing deteriorating effects on the aircraft engine. High circumferential swirl flows and inlet flow angularity decrease the aerodynamic performance and the stall margin and increase the rotor blade loading. The current paper is aimed at the investigation of the flow field in the tip clearance region of low-bypass turbofan transonic compressor rotor under nonuniform circumferential flow conditions through numerical simulation using Ansys CFX. The mathematical models based on 1D Mean Line Code and Dynamic Turbine Engine Compressor Code (DYNTECC) are used to analyze the nonuniform inlet swirl flow of the compressor rotor. The mathematical model is limited to compute the multistage compressor characteristics for the compression system and the combustor of a turbine engine. For the single-stage swirl flow analysis current paper focuses on the CFD based results. The results based on CFD show that co-swirl patterns slightly improve the stability range of the compressor; counter-swirl flows diminish it.

Keywords: bulk flow, turbofan transonic compressor, stall margin, stability range, CFD analysis, 1D Dynamic Turbine Engine Compressor Code

DOI: 10.1134/S0015462821010134

NOMENCLATURE

P_{OR}	Inlet stagnation pressure	U	Blade speed
T_{OR}	Inlet stagnation temperature	m_b^0	Mass flow rate at rotor inlet
P_s	Inlet static pressure	$\bar{\omega}_R$	Pressure loss in the blade row
T_s	Inlet static temperature	$\bar{\omega}_{min}$	Minimum profile loss
\dot{i}	Rothalphy	ξ	Flow deviation angle

In analyzing the turbomachine operation both the absolute reference frame fitted to the frame of the machine and the relative reference frame rotating together with the rotor of the machine are used. The fluid velocities observed from the absolute reference frame are called the absolute velocities, while those viewed from the relative reference frame are called relative velocities. The flow enters into the rotor with an absolute velocity of an angle α_1 ; subtracting vectorially the blade speed we obtain the inlet relative velocity directed at an angle β_1 . Relative to the rotor blades, the flow turns to the direction β_2 at the outlet. Adding vectorially the blade speed we obtain the absolute velocity at the rotor outlet directed at an angle α_2 .

The nonuniform distorted inlet flow at the engine face has a broad range of ramification effects on compressor stability and performance. A considerable change in the aerodynamic aircraft engine intake

configurations has been seen since the introduction of stealth aircraft in the aviation industry. The uncertainty of nonuniform inlet flow ingestion and swirl flow at the engine face has risen due to both civil and military aircraft demands of increased turbofan bypass ratio and a decrease in the overall engine length. Earlier, in assessing the compressor stability the inlet swirl distortion and flow angularity were not considered independently, since it was believed that they make only a slight contribution into the inlet flow in the aerodynamic interface plane. At the same time, the flow swirl was previously considered as broadly induced by inlet pressure distortion. The flow swirl was acknowledged as significant inlet distortion during the development phase of *Tornado* fighter aircraft. However, in recent era the introduction of very high bypass ratio turbofan engines and S-shaped intakes requires to investigate individually the swirling flows with the total pressure distortion. The nonuniform circumferential and radial velocity components at the aerodynamic interface plane are referred to as the swirl flow and the flow angularity, respectively. The blade loading can be altered due to an increase or decrease of the local blade incidence angle relative to the velocity components. Different swirl flows are categorized into four groups, i.e., bulk swirl tightly wound vortices, paired swirl, and crossflow swirl. These classifications depend upon the swirl angle, i.e., the angle between the z and θ components of the axial and tangential direction of flow, respectively. The bulk swirl flow approaching the compressor has a constant swirl angle and rotates in one circumferential direction. At the inlet, the bulk swirl has a single vortex, rotating in the rotor direction (co-swirl) or oppositely to the rotor direction (counter-swirl) [1, 2]

Many experimental investigations predominantly performed on *Tornado* aircraft demonstrated that the use of inlet guide vanes can lessen the inlet flow distortion because of the tangential velocity component that turns the inlet flow in the appropriate flow direction. Moreover, the use of variable guide vanes further improves the inlet flow conditions at the desired angle. However, due to an increase in the engine noise, weight, and length, as well as de-icing issues, the use of IGV at the engine front is not always recommended. The effect of distorted inlet swirl on low-pressure compressor performance of twin-spool, two-stage turbofan engine was investigated earlier. The results of that investigation revealed that an increase in the swirl angle decreases the compressor pressure ratio, mass flow rate, and isentropic efficiency [3]. The geometric parameters of a Serpentine jet engine (S-duct) were investigated and strong vortices developed in short length ducts were found to exist in the aerodynamic interface plane [4]. Twin and paired swirl flows were studied on the basis of the compressor characteristic map using the parallel compressor theory and swirl distortion was; it was found that there exists a strong relationship between the swirl flow and the total pressure distortion. To investigate the effect of twin swirl, bulk swirl, and paired swirl flows on the compressor performance in F106 turbofan engine, 1D mean line analysis, parallel compressor theory, and 3D Euler analysis were used [5]. A three-dimensional Turbine Engine Analysis Compressor Code model that solves compressible, time-dependent, and 3D Euler equations embedded with the streamline curvature code was used to investigate the swirl flow effect on the multistage compressor performance. This study showed that, due to co-swirl flow distortion, the compressor blade loading increased significantly. However, the model used is limited to deal with transonic and supersonic flows, when the rotor blade body force obtained from the turbine engine analysis compressor code is independent of the streamline curvature [6]. A three-dimensional unsteady CFD code called CSTALL was utilized to analyze the steady effect of circumferential distortion on the compressor performance. The researchers found that even a single distortion can cause a compressor surge. Therefore, it was not enough to correlate the body force term with the corrected mass flow [7]. Recently a 3D computational model has been utilized, where turbulent heat transfer and viscous terms are added in the 3D Euler equations to overcome the weaknesses of the turbine engine analysis compressor code and CSTALL models [8].

1. PHYSICAL PROBLEM

NASA transonic compressor Rotor 67 is a first stage rotor designed for two-stage fans. Due to its high mass flow rate and designed pressure ratio, it has been widely researched in the aerospace industry. In [9], laser anemometer measurements in a transonic axial flow fan rotor were performed in NASA Lewis Research Center to propose the Rotor 67 geometry at designed tip clearance of 1.016 mm. In [1], swirl distortion was investigated and its adverse effect on the engine performance of turbofan compressor Rotor 67 was established. The case of 0.6 mm tip clearance was considered in the presence of bulk swirl flow and flow incidence on the blade. These factors reduce the mass-flow rate, thus deteriorating the compressor performance. So far, there is no published work incorporating a comprehensive analysis of the circumferential bulk swirl distortion and high flow angularity effects on the compressor Rotor 67 stability range and stall margin.

In this research one-dimensional mean line compressor and Dynamic Turbine Engine Compressor Code are adopted for an analysis of low bypass multistage compressor characteristics for the compression

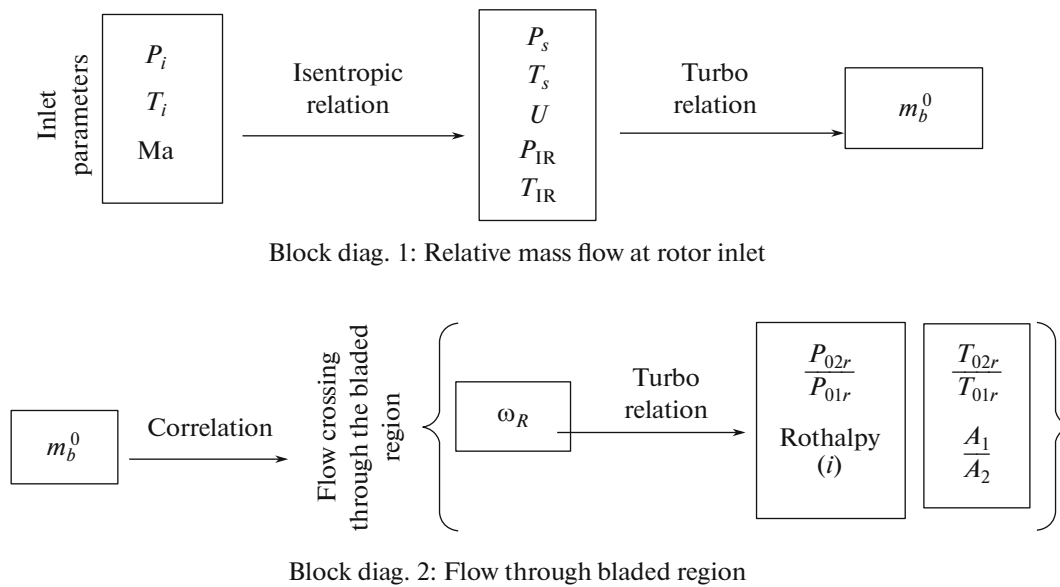


Fig. 1. Block diagram for 1D Dynamic Turbine Engine Compressor Code; (a) relative mass flow at the rotor inlet and (b) flow through the bladed region.

system. For the low-bypass, high-speed first-stage rotor of the transonic two-stage fan, this paper focuses on the CFD-based results. The fan is used extensively in both civil and military short-haul aircraft jet engines. The ingestion of highly distorted and inclined bulk flow is most likely to occur in one-stage transonic compressor Rotor 67. Rotor 67 is investigated to produce a data collection, as a part of a larger project, namely “System Identification Development for Analysis of Transonic Axial Compressor.” This study considers circumferential bulk swirl distortion patterns at 5° , 7° , 10° , 15° , 20° , and 25° and high flow angularity at 85° , 80° , 75° , and 70° because of their practical prevalence. This research study focuses on the engine operability effects due to the distorted inlet circumferential swirl flow ingestion on the transonic compressor rotor without inlet guide vanes and stator blades.

2. COMPUTATIONAL SETUP

The transonic compressor NASA Rotor-67 is composed of 22 blades having 25.7 cm and 24.25 cm tip radii at leading and trailing edges, respectively, as shown in Fig. 1. Three-dimensional coarse, medium, fine, and superfine meshes are generated. For a grid analysis, computations were carried out with 0.4 million to 1.6 million mesh nodes. The results show that the fine hexahedral grid with 0.96 million mesh elements has a decent compromise between computational and experimental results. The three dimensional steady compressible Navier–Stokes equations were solved using the K - ϵ turbulence model. At the rotor outlet boundary the average static pressure is considered, while at the rotor inlet boundary the total pressure of 101325 Pa, the total temperature of 288.15 K, and the flow direction specified for clean inlet flow at designed RPM 16043 are preassigned. The occurrence of a constant swirl angle at the engine inlet is the main characteristic of pure bulk swirl flow. Therefore, the inlet boundary condition is changed accordingly to the following expression for co-swirl flow, counter-swirl flow, and flow angularity at desired circumferential or Cartesian coordinates.

$$\left\{ \begin{array}{l} V_z = \cos\alpha \\ V_r = 0 \\ V_\theta = V_z \tan(\pm\alpha) \end{array} \right\}. \quad (2.1)$$

2.1. One-Dimensional Dynamic Turbine Engine Compressor Code Model

The one-dimensional form of the governing equations and finite-difference method to solve the Navier–Stokes mass, energy, and momentum equations are employed simultaneously in the Dynamic Turbine Engine Compressor Code model. It is used to compute the multistage compressor characteristics

for the compression system and the combustor of a turbine engine. The Dynamic Turbine Engine Compressor Code gives adequate results having a minimum of the compressor rotor data. The set of equations presented below describes the flow in the compressor rotor blade region, and flow crossing the bladed region.

In Fig. 1, the first block diagram shows the flow through the compressor bladed region, when the inlet parameters, such as the total inlet pressure P_i , the total inlet temperature T_i , the inlet flow angle, and the inlet Mach number are known quantities, which determine the static pressure P_s , the static temperature T_s , the blade speed U , the inlet relative total pressure P_{IR} , the inlet relative total temperature T_{IR} , and the relative mass flow at rotor inlet m_b^0 [10, 11]. Precisely the inlet relative total pressure P_{IR} and temperature T_{IR} are the total conditions of the flow that the rotating blade row sees [10]. Furthermore, the relative Mach number M_R is understood to mean the Mach number based on the local speed of sound at the ambient temperature. The coefficient of total pressure loss relative to the blade row $\bar{\omega}_R$ is calculated by correlation equations, as shown in the following block diagram 2 of Fig. 1

$$P_{IR} = P_s \left(1 + \frac{(\gamma - 1)}{2} M_R^2 \right)^{\left(\frac{\gamma}{\gamma - 1} \right)}, \tag{2.2}$$

$$T_{IR} = T_s \left(1 + \frac{(\gamma - 1)}{2} M_R^2 \right), \tag{2.3}$$

$$m_b^0 = m^0 \frac{\sqrt{T_{IR}}}{P_{IR} A}. \tag{2.4}$$

Therefore,

$$\rho = \frac{P_o \left(1 + \frac{(\gamma - 1)}{2} M_R^2 \right)^{-\left(\frac{\gamma}{\gamma - 1} \right)}}{RT_o \left(1 + \frac{(\gamma - 1)}{2} M_R^2 \right)^{-1}}, \tag{2.5}$$

$$m = \frac{P_o \left(1 + \frac{(\gamma - 1)}{2} M_R^2 \right)^{-\left(\frac{\gamma}{\gamma - 1} \right)}}{RT_o \left(1 + \frac{(\gamma - 1)}{2} M_R^2 \right)^{-1}} AM_R \sqrt{\gamma RT}, \tag{2.6}$$

where A is the area perpendicular to the flow;

$$m_b^0 = M_R \sqrt{\frac{\gamma}{R}} \left(1 + \frac{(\gamma - 1)}{2} M_R^2 \right)^{\frac{-(\gamma + 1)}{2(\gamma - 1)}}. \tag{2.7}$$

To calculate the flow through the bladed region of the compressor rotor the area perpendicular to the flow, the relative total pressure, and the temperature ratio are required. In an axial compressor, the length of the blade and the annulus area between the shaft and the shroud decreases throughout the compressor stage. Therefore, this increases the fluid density, as it is compressed, and a constant axial velocity is kept. The transonic compressor has a three-dimensional flow field. Thus, the total pressure loss coefficient $\bar{\omega}_R$ should be determined numerically. The numerical approach was used to calculate three pressure loss components, i.e., the compressor blade profile loss $\bar{\omega}_p$, the secondary loss $\bar{\omega}_{sec}$ and the shock losses $\bar{\omega}_{sh}$ [12]. Therefore, we have

$$\bar{\omega}_t = \bar{\omega}_p + \bar{\omega}_{sec} + \bar{\omega}_{sh}. \tag{2.8}$$

To calculate the blade profile losses, the flow deviation function and minimum profile loss $\bar{\omega}_{min}$ are calculated as follows [13]:

$$\bar{\omega}_p = f(\xi) \bar{\omega}_{min}, \tag{2.9}$$

$$\bar{\omega}_{min} = \bar{\omega}_{ref} f_{Re} \left[1 + \frac{(i_{min} - i_{ref})^2}{R_{stall}^2} \right], \tag{2.10}$$

$$i_{\min} = i_{\text{ch}} + (i_{\text{stall}} - i_{\text{ch}}) \frac{R_{\text{ch}}}{R_{\text{ch}} + R_{\text{stall}}}. \quad (2.11)$$

The following equation is used to calculate the secondary losses in the blade according to the Howell model [14]

$$\omega_{\text{sec}} = \sigma \left(\frac{\cos \beta_1}{\cos \beta_2} \right)^2 C_D. \quad (2.12)$$

The compressor blade shock losses in the primary and secondary flows are modeled using the following nonisentropic equation [15, 16]

$$\omega_{\text{sh}} = 1 - \frac{\left[\frac{(\gamma + 1) \text{Ma}_e^2}{(\gamma - 1) \text{Ma}_e^2 + 2} \right]^{\frac{\gamma}{\gamma - 1}} \left[\frac{(\gamma + 1)}{2(\gamma - 1)\gamma} \right]^{\frac{1}{\gamma - 1}}}{1 - \left[1 + \frac{(\gamma - 1)}{2} \text{Ma}_1^2 \right]^{\frac{-\gamma}{\gamma - 1}}}. \quad (2.13)$$

The relative compressor blade pressure loss is determined by the formula [17]

$$\omega_r = \frac{1 - \left(\frac{P_{2R}}{P_{01r}} \right)}{1 - \left(\frac{P_s}{P_{1R}} \right)}. \quad (2.14)$$

From the above equation for the relative pressure loss, the relative total pressure is determined as follows:

$$\frac{P_{2R}}{P_{1R}} = 1 - \omega_r \left(\frac{P_s}{P_{1R}} \right) \frac{P_{02r}}{P_{01r}} = 1 - \omega_r \left(\frac{P_s}{P_{01r}} \right). \quad (2.15)$$

Rothalpy is a thermodynamic quantity of a compressible fluid that remains constant over the streamlines. It is conserved over the rotor and stator blades but not over a compressor-stage

$$i = h - w_r u_\theta. \quad (2.16)$$

Here u_θ is the tangential component of the absolute velocity. Furthermore, the particular form of the rothalpy conservation equation depends on the multiple reference frame (MRF). The MRF is formulated by relative and absolute velocity components. In terms of the relative velocity, the rothalpy becomes

$$\nabla(\rho i u_R) = -\nabla(\rho w_R u_\theta u_R) - \nabla(\rho u) + \nabla(\tau \cdot u) + \nabla(\lambda \nabla T) + S_H. \quad (2.17)$$

The temperature ratio in the flow passing through the rotor blade region becomes as follows:

$$\frac{T_{2R}}{T_{1R}} = 1 + \frac{U_2^2 - U_1^2}{2C_p T_{R1}}. \quad (2.18)$$

3. DISCUSSION OF THE RESULTS

3.1. Validation

The CFD-based results for a single-stage transonic compressor rotor were first obtained under the choking conditions and then, by means of gradually rising the outlet average static pressure, for the near-stall conditions. Thus, the compressor rotor characteristic graph was determined. The near-stall point was predicted at the last stable condition of Rotor 67. Figures 2a and 2b show the characteristic maps that present the normalized mass flow rate versus the pressure ratio and the adiabatic efficiency of the compressor, respectively, at the designed RPM and TC of 1.016 mm. The results illustrate good agreement between the computational and NASA experimental results [9, 18, 19]. The computational results show a 0.3% difference in the mass flow rate under the designed conditions from the NASA experimental results, which is reasonably encouraging.

3.2. Co-Swirl Flows

Figures 3a–3c show the characteristic map, the stall margin, and the stability range of the co-swirl flow, respectively, at 5°, 7°, 10°, 15°, 20°, 25°, and 30°. These data allow one to determine the optimal operating

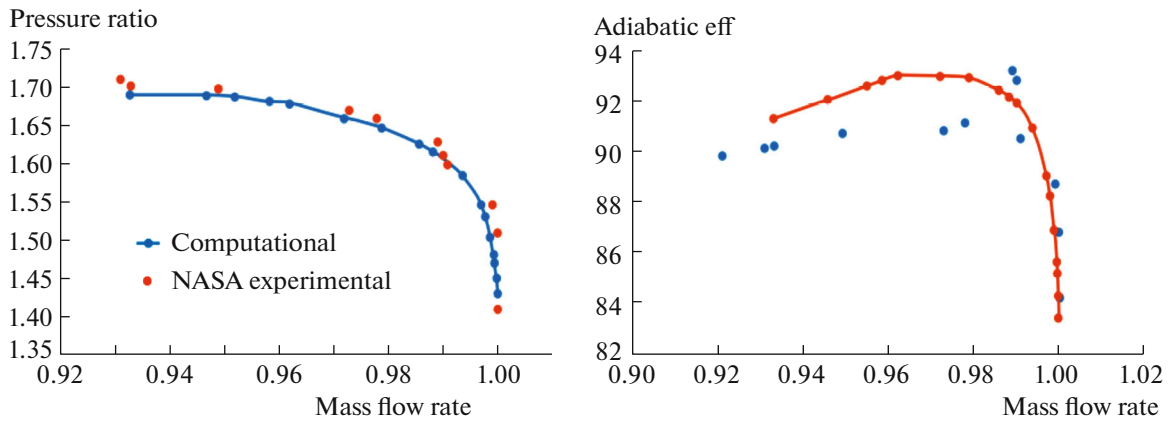


Fig. 2. Characteristic maps [18].

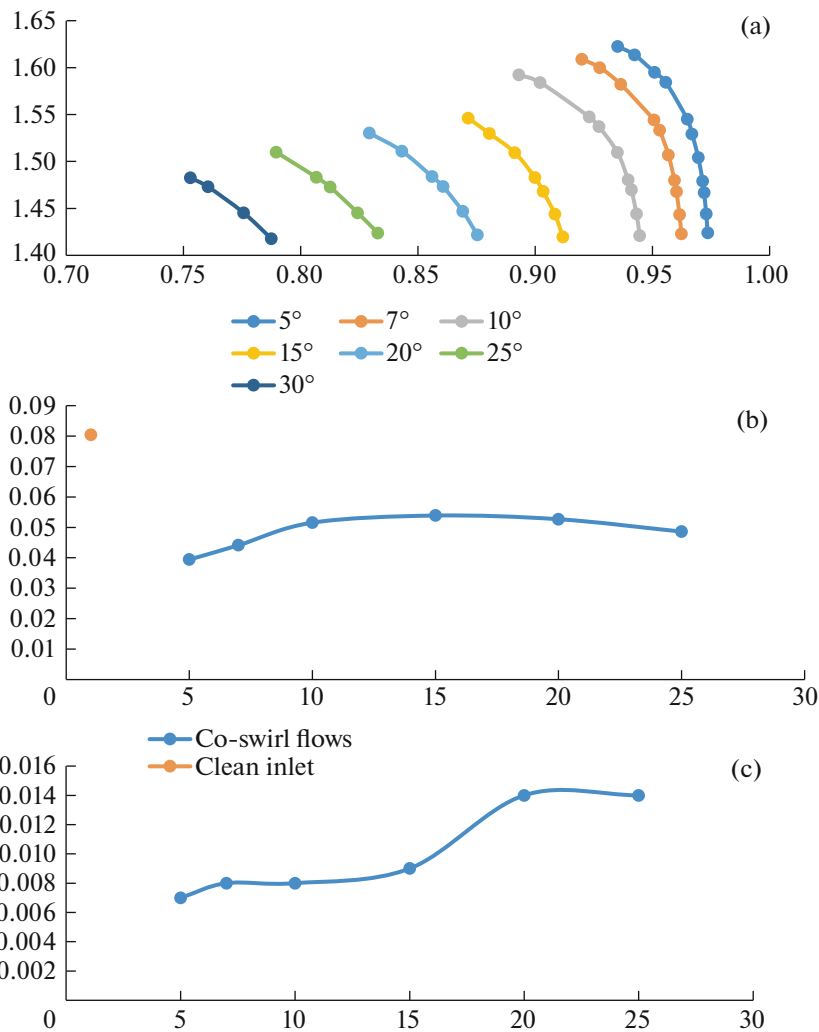


Fig. 3. Co-swirl flow performances: (a) 3D characteristic map, (b) stall margin comparison, and (c) stability margin comparison.

conditions. The results show that the co-swirl flow increases the stall margin and stability range of turbofan transonic compressors at a specific limit. Whereas, it starts to decrease them after 25° co-swirl flows.

Figure 4a shows the pressure blade loading at near stall point of 80% rotor blade span at designed RPM. The scales chosen in each figure are kept the same for the better comparison and visualization of results:

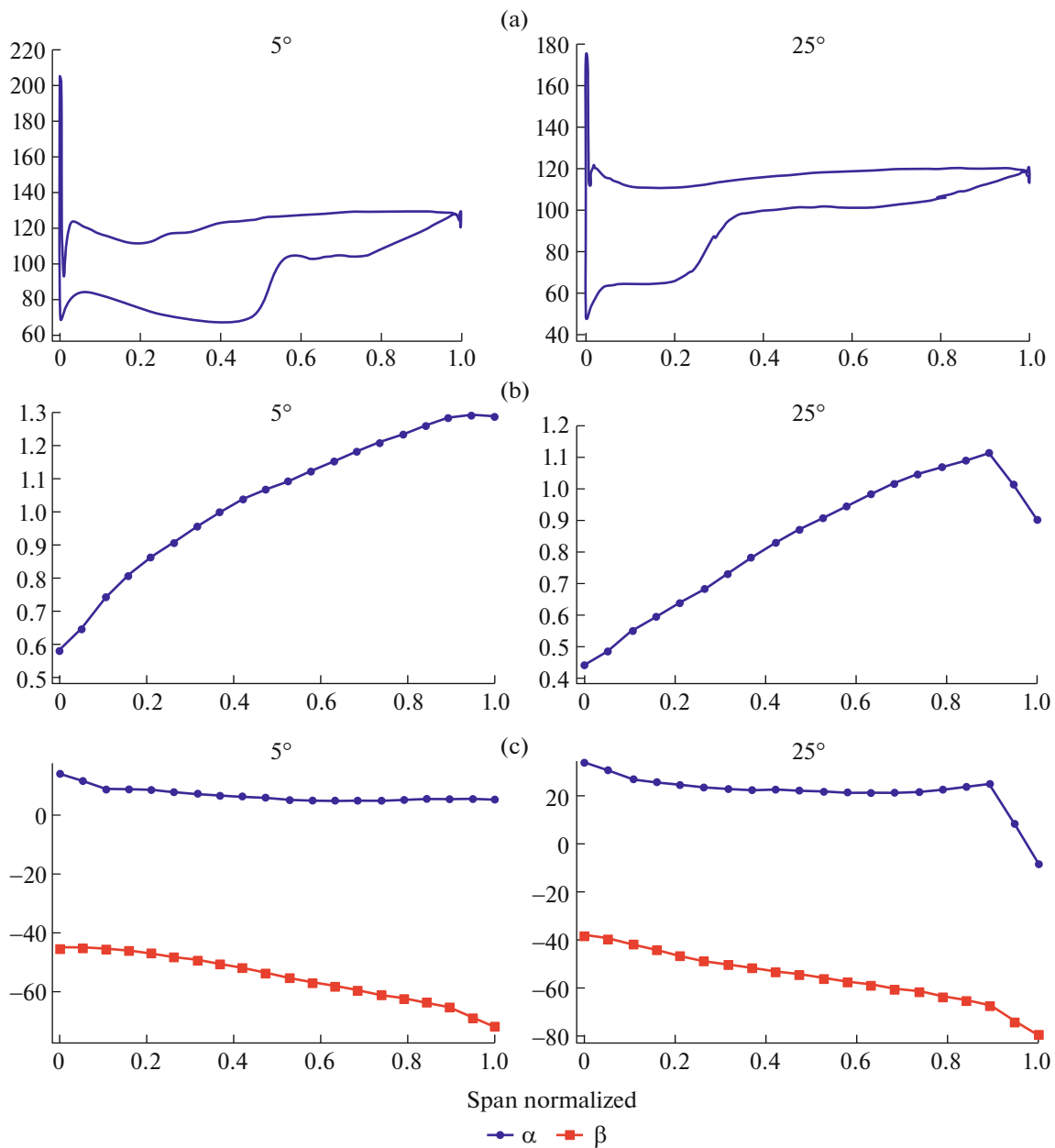


Fig. 4. Co-swirl flow behavior for near stall conditions: (a) pressure blade loading at 80% span, (b) relative Mach number at 80% span, (c) spanwise plot of α and β angles at the leading edge of the blade, and (d) velocity vector at 80% blade span.

here, points 0 and 1 correspond to the leading and trailing edges at the streamwise location. The curve joining the higher pressure points corresponds to the pressure side and that joining the lower pressure points indicates the suction side of the compressor rotor blade. At the leading edge of the blade (LE), the peak pressure load indicates the stagnation point, where the fluid is stagnant for a short period. The figure shows that the compressor rotor blade has a maximum stagnation point at 5° co-swirl and it decreases at higher swirl flows. At 5° co-swirl, at about 50% of blade chord a sudden increase in the static pressure at the suction side of the blade is observed. At the same time, an increase in the swirl angle up to 25° co-swirl leads to an earlier increase in the static pressure along blade chord, which causes the flow deceleration and an increase of entropy.

Figure 4b shows the 80% spanwise distribution of the relative Mach number at LE at near stall point and the designed RPM. The results indicate that at 5° co-swirl the Mach number is nearly 0.55, which

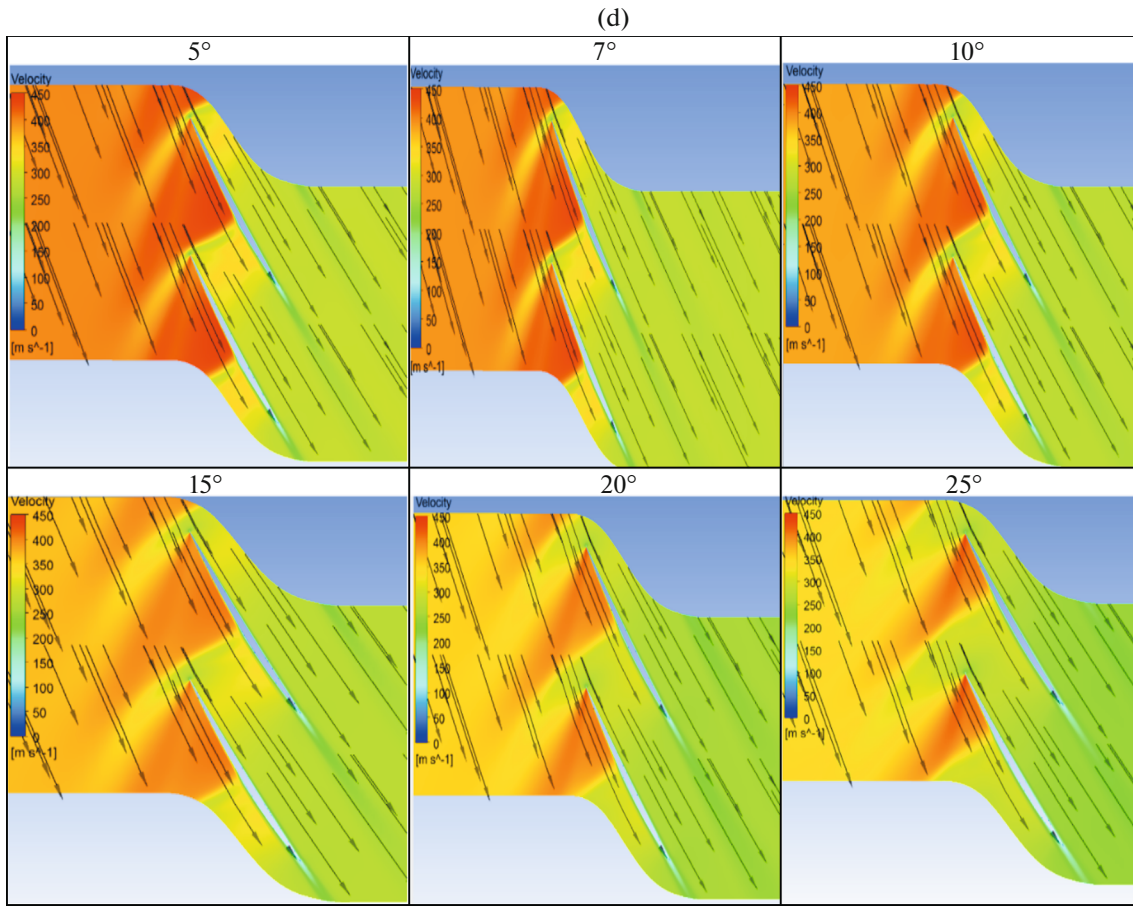


Fig. 4. (Contd.)

decreases at higher swirl flows. A sudden drop of the Mach number can be seen at 25° co-swirl and above near the leading edge of the blade chord. This shows the presence of shock waves at the higher inlet swirl angles. Usually, the circumferential nonuniformity is considered as more severe, since it significantly affects the incidence angle. In the absence of guide vanes, the flow entering the compressor is likely to have some amount of swirl. This swirl may get amplified under certain conditions, leading to severe inflow distortion.

Figure 4c shows the absolute angle α and the relative angle β along the span of various airfoils. The results show that the former angle does not change considerably along the span with exception of the region near the tip clearance. At the same time, due to the distorted inlet swirl flow, the relative angle β varies significantly. The relative angle β decreases due to an increase of swirl flow angle. This improves the compressor stability and performance.

Figure 4d shows the formation of strong oblique shock waves at higher swirl angles near the blade leading edge, which results in a sudden drop of relative Mach number at the blade leading edge, as shown in Fig. 4b, and flow separation.

3.3. Counter Swirl Flows

Figures 5a– 5c show the characteristic map, the stall margin, and the stability range of the counter swirl flow at 5°, 7°, 10°, 15°, 20°, and 25° which allow one to determine the optimal operating conditions. The results show that the counter swirl flow slightly increases the stall margin up to 10°, but with further increase in the swirl angle it starts to decrease. As for the stability range of the turbofan transonic compressor, this decreases due to the counter swirl flow.

Figures 6a and 6b show the pressure blade loading at 80% rotor blade span in the case of the counter swirl flow at near stall point and at designed RPM and spanwise distributions of the relative Mach number

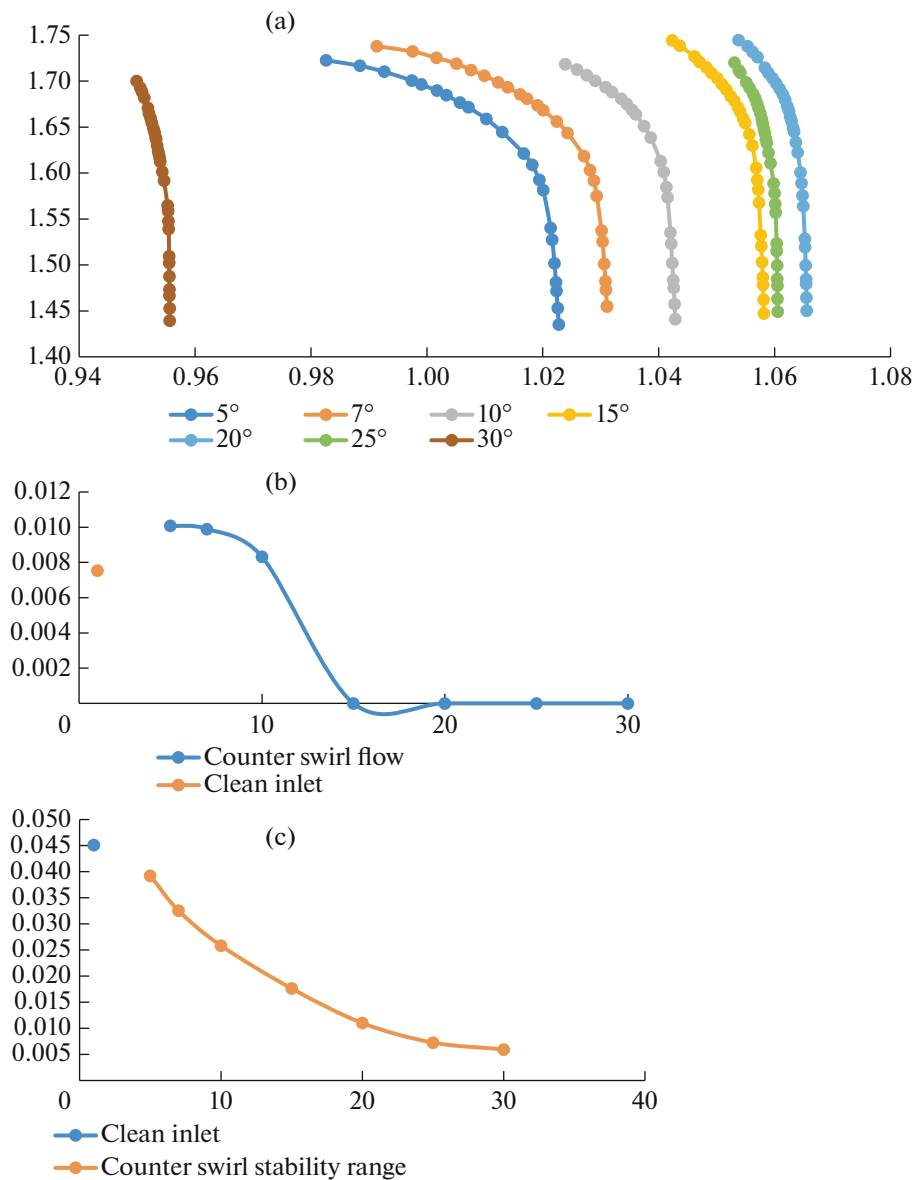


Fig. 5. Counter-swirl flow performances: (a) 3D characteristic map, (b) stall margin comparison, and (c) stability margin comparison.

at the leading edge of the rotor blade. The results show that the compressor rotor blade has a maximum stagnation point pressure at 5° counter swirl and it decreases at higher swirl flows. At 5° counter swirl, a sudden increase of the static pressure is observed at about 10% of the blade chord at the suction side of the blade. At higher increase in the counter-swirl angle the static pressure increases farther along the chord, which intensifies the flow near the blade tip and, therefore, decreases the entropy. Figure 6c shows the distributions of the absolute angle α and the relative angle β along the span for various counter-swirl angles.

The results show that, due to the distorted inlet swirl flow, the relative angle β varies significantly. The value of this angle increases with increase in the counter-swirl flow angle. This deteriorates the compressor stability and performance.

Finally, Fig. 6d presents the formation of weak oblique shock waves at higher counterswirl angles of blade LE, which results in an increase of the relative Mach number at LE, as shown in Fig. 6b. At the trailing edge of the blade, low-velocity regions are dominant at higher counter swirl flows.

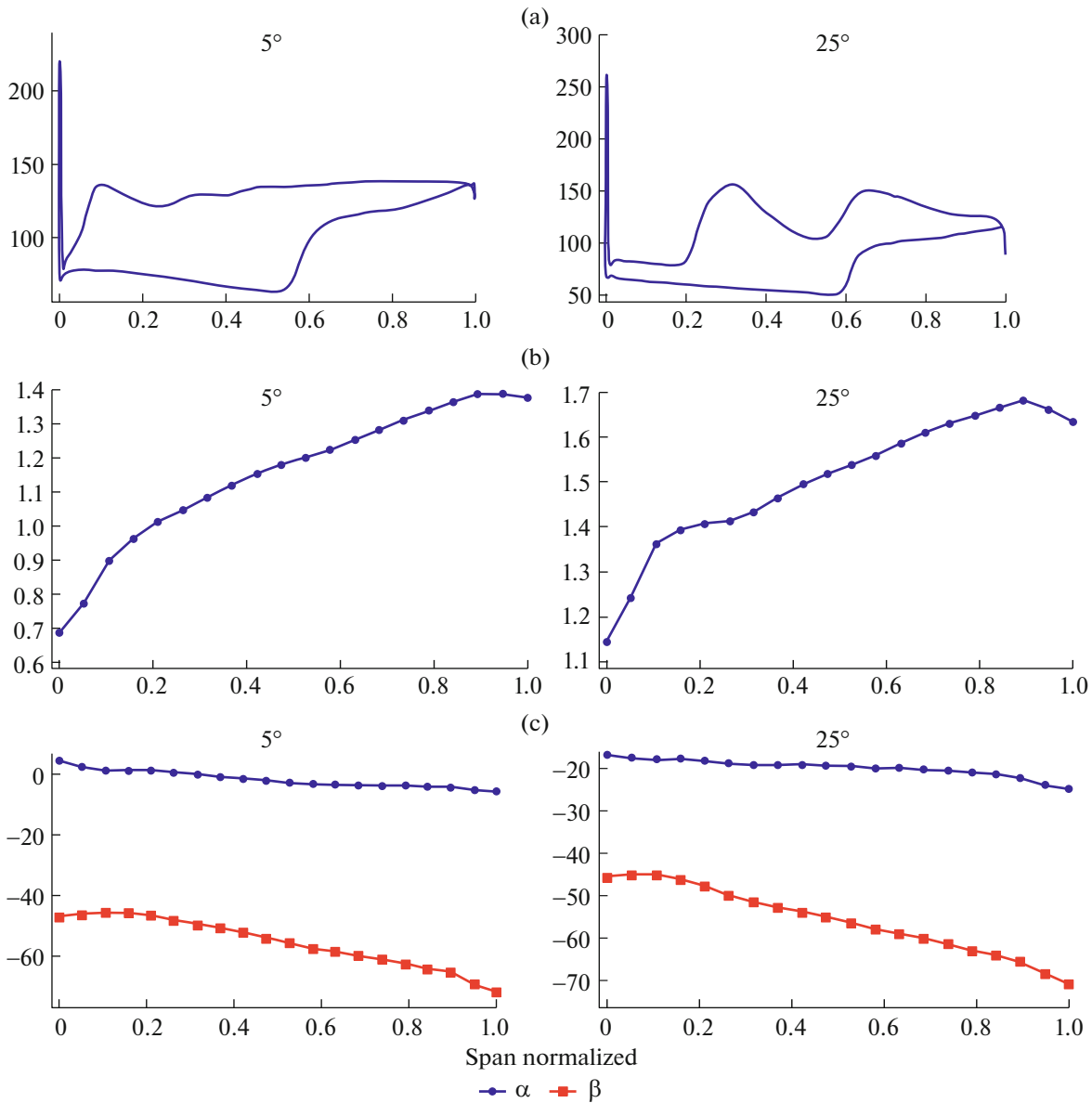


Fig. 6. Counter-swirl flow behavior: (a) pressure blade loading at 80% span, (b) relative Mach number at 80% span, (c) spanwise plot of α and the β angle at the leading edge of the blade, and (d) velocity vector at 80% blade span.

3.4. Flow Angularity

Figure 7a shows the characteristic map in the case of flow angularity. The results show a decrease in the mass flow rate at a higher incidence angle. This causes a decrease in the stage efficiency and the stall margin. Figure 7b shows the pressure blade loading at 80% span of the blade. Here points 0 and 1 are termed as leading and trailing edges at the streamwise location. The curve joining the higher pressure points indicates the pressure side and that joining the lower pressure points indicates the suction side of the compressor rotor blade. At LE the peak pressure load indicates the stagnation point, where the fluid is stagnant for a short period. The results show the separation of flow from the boundary layer at a higher incidence angle than usually. Furthermore, the formation of first shock waves at the leading edge of the blade and ingested second shock wave at the trailing edge of the blade leads to boundary layer separation. Figures 7c and 7d show the spanwise distributions of the relative Mach number at the leading edge of the blade and the velocity vector at 80% span of the blade. The results indicate that at 85° angular flow the Mach number is nearly 0.6 and it decreases at higher angularities, i.e., at 70°. At the same time, at the TE

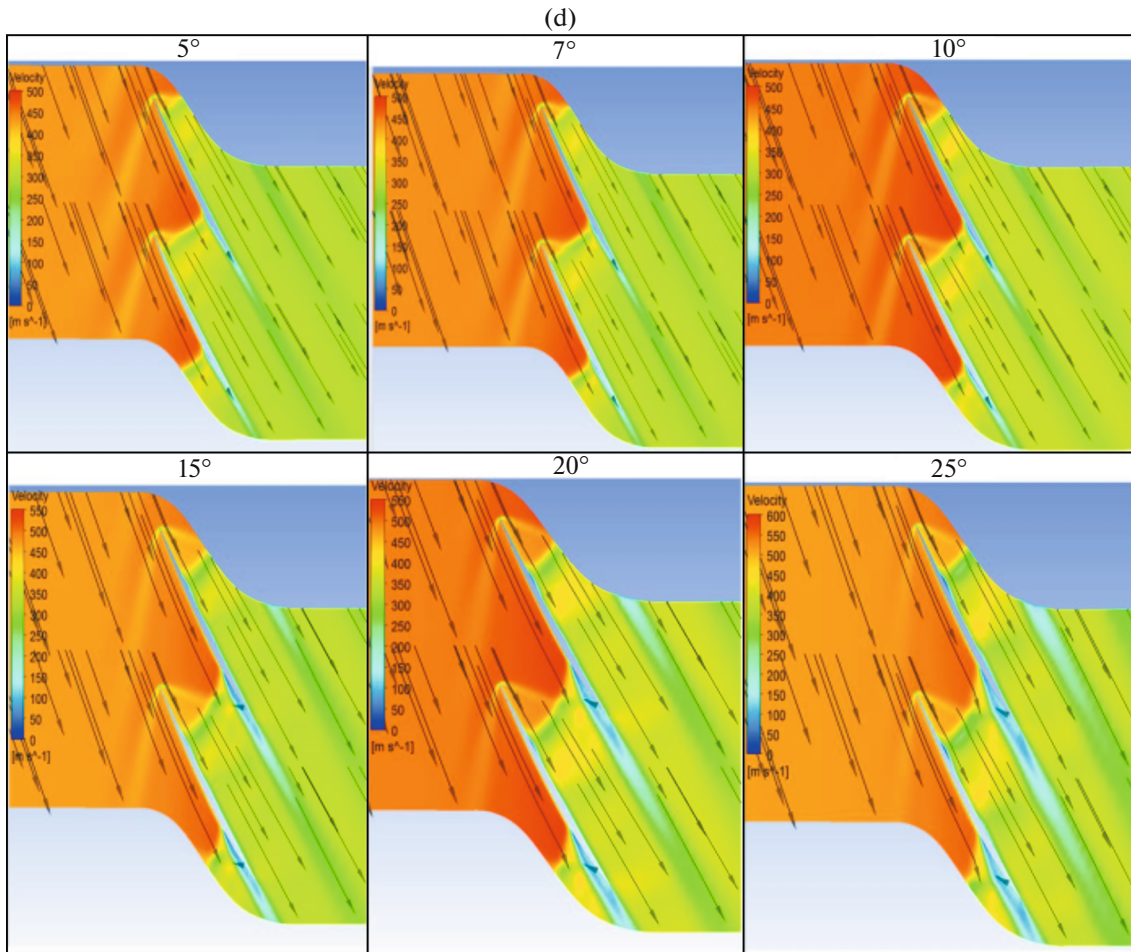


Fig. 6. (Contd.)

of the blade a decrease in the Mach number is observable at higher angularities. This shows the presence of shock waves at higher angular flows. Figure 7d shows the presence of strong shock waves at 70° flow angularity. This can lead to flow separation from the LE of the blade.

SUMMARY

The current paper focuses on the effect of inlet flow distortion on the performance and stability of the turbofan transonic compressor rotor. Numerical simulations with circumferential bulk flow distortion patterns and flow angularity are carried out. The following conclusions are drawn because of this study.

Dynamic Turbine Engine Compressor Code can use Mean Line Code and determine the compressor stage characteristics without the use of characteristic maps.

The counter swirl distorted inlet flow decreases the stability range of the transonic compressor rotor. It shifts the characteristic map of the compressor to the right and upward. At the same time, the co-swirl inlet distortion increases the compressor stability and stall margin, as it shifts the characteristic map to the left and downward.

In contrast to the co-swirl flow, the compressor rotor higher pressure ratio is achieved in counter swirl flow because of the greater work done by the rotor. This also increases the relative Mach number and, therefore, the counter swirl flow decreases the compressor stability.

In the case of inflow angularity, when the absolute angle is higher than the normal axial direction, the separation of flow from the boundary layer is seen. Furthermore, the formation of shock waves at the lead-

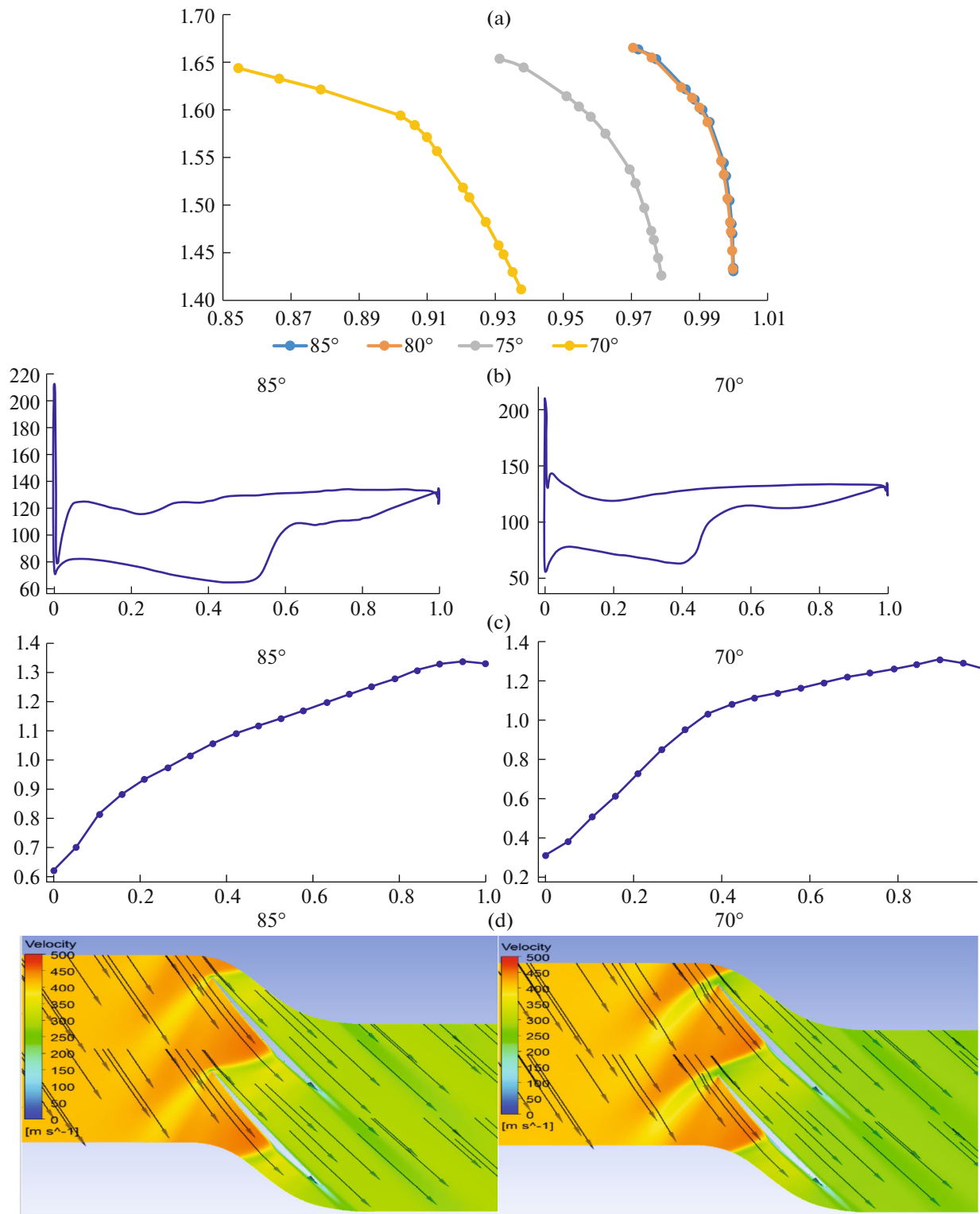


Fig. 7. Flow angularity behavior: (a) Characteristic map, (b) Pressure blade loading at 80% span, (c) Relative Mach number at 80% span, and (d) Velocity vector at 80% blade span.

ing edge of the blade and ingested second shock wave at the trailing edge of the blade are observable. This causes boundary layer separation.

REFERENCES

1. A. Mehdi, *Effect of Swirl Distortion on Gas Turbine Operability*, School of Engineering Power and Propulsion Department, Cranfield University, May 2014.
2. Y. Sheoran and B. Bouldin, "Inlet flow angularity descriptors proposed for use with gas turbine engine," in: *Proceedings of Society of Automotive Engineer (SAE) Technical Conference, India, 2002*.
3. W. Pazur and L. Fottner, "The influence of inlet swirl distortions on the performance of a jet propulsion two-stage axial compressor," *J. Turbomachinery* **113**, 233–240 (1991).
4. K. M. Loeper and P. I. King, "Numerical investigation of geometric effects on performance of S-ducts," in: *IAA 2009-713, 47th AIAA Aerospace Sciences Meeting Including the New Horizons Forum and Aerospace Exposition, Orlando, Florida, January 2009*.
5. M. Davis and A. Hale, "A parametric study on the effects of inlet swirl on compression system performance and operability using numerical simulations," in: *GT2007-27033, ASME Turbo Expo 2007: Power for Land, Sea, and Air, Montreal, Canada, May 2007*.
6. A. Hale and W. O'Brien, "A three-dimensional turbine engine analysis compressor code (TEACC) for steady-state inlet distortion," *ASME J. Turbomachinery* **4**, 422–430 (1999).
7. R. V. Chima, "A three-dimensional unsteady CFD mode of compressor stability," *ASME Journal of Turbomachinery*, 1157–1168 (2008).
8. J. Guo and J. Hu, "A three-dimensional computational model for inlet distortion in fan and compressor," *J. Power Energy* **232**, 1–13 (2018).
9. A. J. Strazisar, J. R. Wood, M. D. Hathaway, and K. L. Suder, "Laser anemometer measurements in a transonic axial-flow fan rotor," NASA Scientific and Technical Division, Lewis Research Center, Cleveland, Ohio, 1989.
10. S. L. Smith, "One-dimensional mean line code technique to calculate stage-by-stage compressor characteristics," University of Tennessee, Knoxville, 1999.
11. R. N. Pinto, R. Nivea, A. Afzal, L. Vinson, D'Souza, and Z. Ansari, "A review of state of the art archives of computational methods in engineering," in: *Archives of Computational Methods in Engineering, Barcelona, Spain, 2016*.
12. J. F. Hu, X. Ch. Zhu, H. OuYang, X. Q. Qiang, and Zh. H. Du, "Performance prediction of the transonic axial compressor based on the streamline curvature method," *J. Mechanical Science and Technology* **12**, 3037–3045 (2011).
13. I. Templalexis, P. Pilidis, V. Pachidis, and P. Kotsiopoulos, "Development of a 2D compressor streamline curvature code," in: *SME Turbo Expo, Power for Land, Sea, and Air, Barcelona, Spain, 2006*.
14. C. Schwenk, G. W. Lewis, and M. J. Hartman, "A preliminary analysis of the magnitude of shock losses in transonic compressors," NASA Paper, 1957.
15. W. C. Swan, "A practical method of predicting transonic compressor performance," *J. Eng. Power*, 322–330 (1961).
16. N. J. Fredrick, "Investigation of the effects of inlet swirl on compressor performance and operability using a modified parallel compressor model," University of Tennessee, Knoxville, 2010.
17. R. H. Aungier, "Axial-flow compressor: A strategy for aerodynamic design and analysis," in: *ASME*, New York, 2003.
18. M. U. Sohail, H. R. Hamdani, and K. Parvez, "CFD analysis of tip clearance effects on the performance of transonic axial compressor," *Fluid Dynamics* **55**(1), 133–144 (2020).
19. M. U. Sohail, M. Hassan, H. R. Hamdani, and K. Parvez, "Effects of ambient temperature on the performance of turbofan transonic compressor by CFD analysis and artificial neural networks", *Engineering, Technology & Applied Science Research* **9**(5), 4640–4648 (2019).
20. B. Bouldin and Y. Sheoran, "Impact of complex swirl patterns on compressor performance and operability using parallel compressor analysis ISABE2007-1140," in: *18th International Symposium on Air Breathing Engines, Beijing, China, September 2007*.
21. M. Davis, D. Beale, and Y. Sheoran, "Integrated test and evaluation techniques as applied to an inlet swirl investigation using the F109 gas turbine engine," in: *GT2008-50074, ASME Turbo Expo 2008: Power for Land, Sea, and Air, Berlin, Germany, June 2008*.
22. G. R. Miller, G. W. Lewis, and M. J. Hartmann, "Shock losses in transonic rotor rows," *J. Eng. Power*, 235–242 (1961).
23. Y. S. B. Bouldin, "Impact of complex swirl patterns on compressor performance and operability using parallel compressor analysis," in: *ISABE2007-1140, 18th International Symposium on Air Breathing Engines, Beijing, China, 2007*.